Multidisciplinary Research Journal
ISSN: 3049-2718 (Print)

Volume 1, Issue 2, 2025
April – June 2025

Review

Technique of Synthesis of Anisotropic Shaped Plasmonic Nanoparticles

Subrata Biswas [1], Pathik Kumbhakar [1]*

[1] Nanoscience Laboratory, Dept. of Physics, National Institute of Technology Durgapur, 713209 West Bengal, India.
* Correspondence: nitdgpkumbhakar@yahoo.com

Scopus Author ID 6701424407

Received: 16 December 2024; Accepted: 25 March 2025; Published: 28 April 2025

Abstract: Anisotropic nanoparticles have attracted considerable attention for their distinctive shape-dependent optical, electronic, and catalytic properties, making them valuable across diverse applications, including medicine and nanotechnology. This abstract presents an overview of synthesis techniques used to produce anisotropic nanoparticles with controlled shapes, sizes, and compositions. Various methods, including chemical reduction, seed-mediated growth, and template-assisted approaches, are discussed in terms of their efficiency, reproducibility, and scalability. Emphasis is placed on understanding the role of surfactants, reducing agents, and reaction conditions in driving anisotropic growth. Additionally, recent advancements in green synthesis methods highlight the shift towards environmentally friendly procedures. The review provides insights into how precise control over nanoparticle anisotropy enhances their functional properties and enables their targeted applications in photonics, biomedicine, and catalysis. The findings underscore the potential of these techniques to advance the design and fabrication of next-generation anisotropic nanomaterials.

Keywords: Anisotropic nanoparticles; Plasmonic nanoparticles; Synthesis Techniques; Surfactants

1. Introduction

Nanoparticles with anisotropic shapes [1] [2] such as rods [3], triangles [4], stars [5], and prisms [6] have become a central focus in nanoscience because of their distinctive physical and chemical properties. Unlike isotropic nanoparticles, whose properties primarily depend on size, anisotropic nanoparticles exhibit shape-dependent behavior that significantly enhances their optical [7], electronic [8], and catalytic functionalities [9]. This shape anisotropy opens up a spectrum of uses, with a specific focus on targeted drug delivery [10], biomedical imaging [11], environmental sensing [12], and photocatalysis [13].

Anisotropic nanoparticles offer several advantages over regular, isotropic nanoparticles due to their directional properties, which allow for enhanced control and functionality. Here are some key points of importance:

1.1. Tunable Optical Properties

Anisotropic nanoparticles, such as rods or prisms, exhibit unique optical behaviors [14] because they interact differently with light along their various dimensions. This results in strong surface plasmon resonances (SPRs) [15] [16] that can be tuned by adjusting their shape and size [17] [18]. These SPRs enable applications in sensing [12], imaging [11], and photothermal therapy [19], where precise control over light absorption and scattering [20] [21] is essential.

1.2. Enhanced Catalytic Activity

Many anisotropic nanoparticles possess highly active crystal facets and edges that make them excellent catalysts [22]. The sharp tips and high surface-to-volume ratio [23] of anisotropic particles, such as nanostars or nanorods, expose more reactive sites [24], increasing the efficiency and selectivity of catalytic reactions. This is valuable in environmental applications and industrial processes where efficient catalysis is needed.

1.3. Targeted Biological Interactions

The unique shape of anisotropic nanoparticles improves their interaction with biological systems, viz., nanorods and nanostars are more easily taken up by cells than spherical particles, which enhance their effectiveness in drug delivery and imaging. Their shape can also influence circulation time and biodistribution in the body, making them more effective in biomedical applications like cancer treatment [25].

1.4. Improved Mechanical and Magnetic Properties

Certain anisotropic shapes, like nanowires and nanotubes, exhibit mechanical properties that are useful in flexible electronics [26] and structural nanocomposites [27]. Similarly, anisotropic magnetic nanoparticles, such as iron oxide nanorods, show directional magnetic properties [28], making them suitable for magnetic data storage [29] and targeted magnetic hyperthermia [30] in cancer treatment.

1.5. Greater Stability and Environmental Control

Some anisotropic nanoparticles exhibit greater thermal and chemical stability, which enhances their robustness under different environmental conditions. This provides benefits for applications where long-term stability is crucial, like solar cells [31], sensors [32], and coatings [33].

1.6. Enhanced Sensitivity in Sensing Applications

Anisotropic nanoparticles are highly sensitive to changes in environment, such as pH [16], temperature [34], and the presence of specific biomolecules [35]. This sensitivity is particularly useful in sensor technology, where these particles can provide precise and real-time monitoring of chemical or biological changes, making them ideal for environmental monitoring and diagnostics [36] [37].

1.7. Multifunctionality for Advanced Applications

Due to their shape-dependent properties, anisotropic nanoparticles can often perform multiple functions. For example, gold nanorods can function both as contrast agents for imaging [38] and as therapeutic agents in photothermal therapy [39]. This multifunctionality is valuable in fields that require integrated solutions, like nanomedicine and theragnostic [40].

The synthesis of anisotropic nanoparticles is a complex yet exciting area of research, involving the precise manipulation of growth processes [41] to achieve specific geometries and aspect ratios [42]. Multiple synthesis techniques have been devised to achieve regulated

anisotropy in these nanoparticles, including chemical reduction techniques [43], seed-mediated growth [44], and template-assisted synthesis [45]. Each method requires careful control of parameters, including surfactant types [46], reducing agents [44], and reaction temperatures [44], which together influence the nucleation and growth processes [47]. Recent advancements in synthesis have further enabled the production of anisotropic nanoparticles through more eco-friendly and sustainable routes [48]. The development of green synthesis methods has opened new avenues for producing these materials with reduced environmental impact, thereby expanding their potential applications. This review explores key synthesis techniques for anisotropic nanoparticles, highlighting the underlying mechanisms that drive anisotropic growth, as well as recent innovations aimed at enhancing efficiency, scalability, and environmental compatibility. The controlled synthesis of anisotropic nanoparticles holds immense promise for advancing nanotechnology applications and enabling future breakthroughs in materials sciences.

2. Synthesis Techniques

Nanoparticle synthesis is generally divided into two primary approaches: the top-down approach [49] and the bottom-up approach [49]. Each of these approaches utilizes different methods to control the size, shape, and properties of nanoparticles and has unique advantages and limitations.

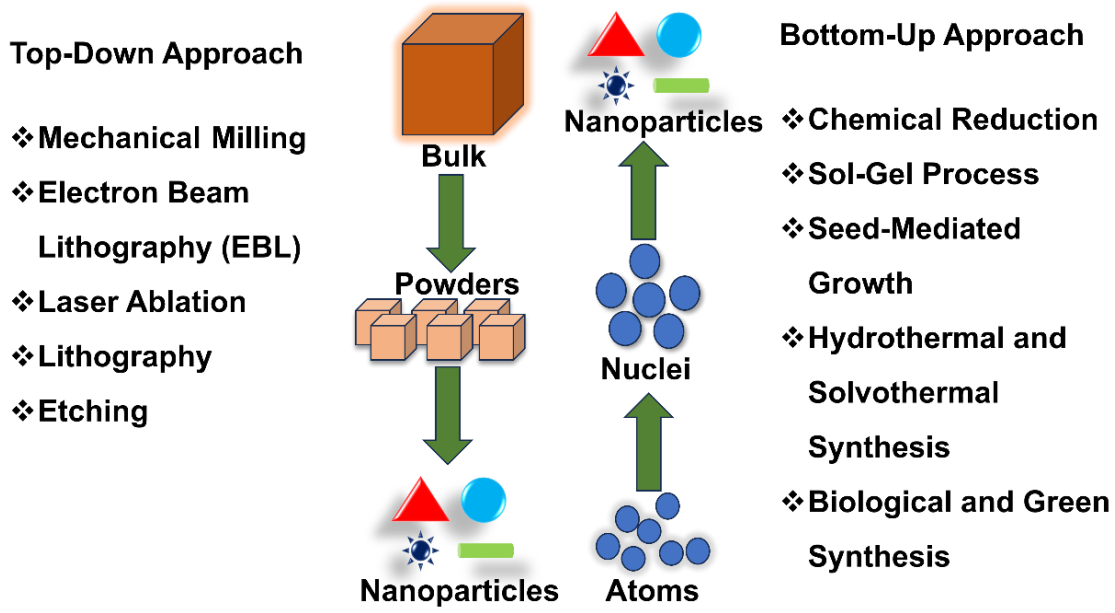

Figure. 1. A schematic illustrating the top-down and bottom-up approaches for nanoparticles' synthesis.

2.1. Top-down Approach

Nanoparticle formation via the top-down method relies on the physical or mechanical breakdown of bulk materials, exemplified by milling, grinding, and lithography [49]. This approach is particularly useful for fabricating specific shapes and sizes but has limitations regarding the precision of size control at the nanoscale. Some commonly used top-down methods of syntheses of nanoparticles are described below, briefly.

Commonly used Top-down Methods:

2.1.1. Mechanical Milling

Bulk materials are mechanically ground to break down particles to the nanoscale [50] [51]. This method is commonly used for metals and oxides but can introduce defects in the particles and has limitations in achieving uniform sizes.

2.1.2. Laser Ablation

A high-energy laser [52] is directed at a solid material, causing the material to evaporate and condense into nanoparticles. This technique allows control over particle size by adjusting the laser's energy and frequency, but it is generally low-yield and costly.

2.1.3. Lithography

Lithographic techniques, such as electron-beam lithography [53], are used to create precise nanoscale patterns and particles on a substrate [54]. This method allows high precision in shape and size but is typically used for creating two-dimensional nanoparticle arrays rather than bulk synthesis and can be labor-intensive and costly.

2.1.4. Etching

Chemical or physical etching is used to remove material from a bulk substrate to achieve nanoscale features. This is a common technique in semiconductor fabrication [55], though its high cost limits its application in large-scale nanoparticle synthesis [56].

Advantages of top-down approach

There are a lot of advantages of top-down approach for syntheses of metal nanoparticles and some of those advantages and limitations of this technique are mentioned below [60]-[67].

I. This technique can be employed suitably to achieve some good control over particle shape and size, which are required for certain applications.
II. Potentially high purity of nanoparticles can be synthesized, as contamination is reduced by starting with high-quality bulk material.
III. This technique is suitable for synthesizing larger particles or particles that require specific geometries.

Limitations

I. Often less precise for extremely small nanoparticles (<10 nm).
II. Higher chance of introducing defects, internal stress, or impurities due to mechanical and thermal stresses.
III. Higher energy and material waste, making it less efficient and environmentally friendly.

2.2. Bottom-Up Approach

In the bottom-up approach [57] [58], nanoparticles are created by assembling atoms or molecules into larger structures. This approach is commonly used for synthesizing nanoparticles in solution and allows for better control over the composition and size distribution, especially at smaller scales. Some commonly used bottom-up methods are described below.

Commonly used bottom-up methods

2.2.1. Chemical Reduction

Metal ions in solution are chemically reduced [59] [60] to form metal nanoparticles. This is widely used for gold, silver, and other metal nanoparticles, where reducing agents (like sodium borohydride) facilitate the growth of nanoparticles. Surfactants [59] [60] can be added to control shape and size.

2.2.2. Sol-Gel Process

In this method, a solution of metal alkoxides or salts undergoes hydrolysis [61] and condensation reactions [62] to form nanoparticles. This technique is widely used to produce oxide nanoparticles and allows good control over size, porosity, and purity.

2.2.3. Seed-Mediated Growth

Pre-formed "seed" nanoparticles [63] are used as nucleation sites to grow larger particles by adding more precursor material in a controlled manner. This approach is commonly used to make anisotropic shapes like rods or stars, as shape-controlling agents' direct growth along specific dimensions [64].

2.2.4. Hydrothermal and Solvothermal Synthesis

Precursors are dissolved in water (hydrothermal) [65] or organic solvents (solvothermal) [59] and subjected to high pressure and temperature. These conditions facilitate the controlled growth of a variety of nanoparticles with different shapes and high crystallinity.

2.2.5. Synthesis Biological and Green Synthesis

Organisms like bacteria, fungi, and plants can synthesize nanoparticles by naturally reducing metal ions. This eco-friendly approach [66] [67] avoids toxic reagents and provides biocompatible nanoparticles but is limited by the rate of synthesis and variability in size and shape. Some advantages and limitations of this technique are also mentioned below [66] [67].

Advantages of bottom-up approach

I. High control over nanoparticle size and morphology, especially at the sub-10 nm level.
II. Often more environmentally friendly, especially in green synthesis.
III. Scalability, particularly in chemical reduction and sol-gel methods.

IV. Ability to incorporate a wide range of materials, including organic and composite nanoparticles.

Limitations

I. Aggregation can be a problem in solution-based synthesis, which affects stability and uniformity.
II. Limited control over large-scale shapes or structures compared to lithography in top-down methods.
III. Some methods can require longer processing times or additional steps for purification.

3. Chemical and Solvothermal Syntheses Techniques in Creating Anisotropic Nanostructures

Due to the unique physical and chemical properties Ag nanostructures has gained noteworthy attention in many practical applications. These practical applications demand the controlling over size and shape of Ag nanostructures as the Plasmonic behavior depends on the size, shape, and surrounding environment of the Ag nanostructures. For the synthesis of Ag nanostructures two main approaches, namely chemical and physical methods are used extensively. The ability to achieve desired shape and size makes chemical synthesis the widely accepted method for Ag nanostructure production. In chemical synthesis techniques primarily a given Ag precursor is reduced by a reducing agent and a stabilizing and shape promoting agent has been added simultaneously to obtain desired growth. There are several reports available on literatures on successful synthesis of Ag nanostructures, where Ag nanostructures of desired shape and sized have been obtained by chemical synthesis techniques. Sun and Xia [60] were the first to synthesize monodispersed silver nanocubes in large quantities using the polyol method, where silver nitrate was reduced with ethylene glycol, and PVP dynamically influenced both stability and morphology. The silver nanocubes of tunable sizes of 20-50nm can be achieved by adjusting the molar ratio of $AgNO_3$ to PVP. This report initiated an enormous curiosity among the researchers to explore the possibilities of wet chemistry methods for controlling shapes, sizes and structures of Ag nanostructures [60]. Another shape of the Ag nanostructures which have gained lot of research interest is Ag nanoprism because of its easily tunable absorption property from visible to infrared just by varying its aspect ratio. Among the different Ag nanostructures triangular silver nanoparticles (TNS), and Ag nanoprism have gained huge attention from the research community due to the fact that varying the aspect ratio (side length to thickness) allows for controlled shifting of the absorption band from the visible to the infrared range. Thus lots of efforts have been paid to synthesize TNS and Ag nanoprism of various aspect ratios. Jin *et al.* [68] was the first to synthesize Ag nanoprism in 2001 through photo-induced conversion of the previously prepared spherical Ag nanoparticles by irradiating it with conventional 40-W fluorescent light. Afterwards various synthesis methods are reported where different wavelengths of the light were used to synthesize the Ag nanoprism. It is thought to be the first step towards the successful combination of the light irradiation and chemical reduction which paved the way for the successful synthesis of the Ag nanostructures. On the other hand the Ag nanowire (AgNW) have created a lot of research interest in both academia and industry because of their possible applications in many photonic and electron devices. In

the last three decades researchers have prescribed different synthesis methods to prepare AgNW and most of them are very similar to the strategy adopted in the synthesis of the quantum wires. Initially Ag nanostructures were synthesized using electro-chemical methods but it suffers from the disadvantages of the low yield and non-uniform nature of the synthesized AgNW. However, with the advancement the polyol synthesis methods several researchers have reported the successful synthesis of the uniform high yield synthesis of the AgNW. Sun *et al.* (2023) successfully synthesized uniform silver nanowires (AgNWs) by chemically reducing silver nitrate ($AgNO_3$) with ethylene glycol at a high temperature of 160 °C. The presence of seed particles and polyvinylpyrrolidone (PVP), serving as stabilizing agents, enabled this process. The resulting AgNWs exhibited consistent diameters ranging from 30 to 40 nanometers and impressive lengths reaching up to 50 micrometers. A polyol process has been employed to synthesize silver nanowires. Coskun *et al.* [70] have performed detailed parametric study on the polyol synthesis of the AgNW to investigate the role of temperature, injection rate, molar ratio of PVP and $AgNO_3$, NaCl amount, and stirring rate is on final morphology of the AgNW. In these complex nanostructures of silver, the LSPR resonance shifts to the near-infrared (NIR) which make them an obvious choice for the diagnostic and therapeutic biomedical applications. Thus the synthesis of more complex structures of Ag, like nano-cage and star shaped are carried out by researchers from different branches. Pal *et al.* [71] performed an investigation into the reversible processes of formation and dissolution of silver nanoparticles (Ag NPs) within aqueous solutions containing surfactants. Recently, Oliveira *et al.* [72] synthesized star-shaped Ag nanoparticles using chemical reduction, deposited them onto office paper, and utilized the resulting substrate for analyte detection via SERS.

Hydrothermal and solvothermal synthesis methods are recognized as effective techniques for producing metal nanoparticles with diverse shapes and sizes. The hydrothermal and solvothermal techniques are not new; in the past century they are extensively used in the extraction of element from ore. Hydrothermal synthesis involves chemical reactions in aqueous solutions at temperatures exceeding water's boiling point, whereas solvothermal synthesis utilizes non-aqueous solvents. In this synthesis technique as the temperature is maintained above the boiling points of the liquid used to behave as supercritical fluids which promote the synthesis of the highly crystalline metal nanoparticles. Anisotropic structures can be formed by simply varying the reaction time or temperature. The hydrothermal/solvothermal process has other advantages too like (i) it is a green synthesis technique as it is performed on closed system conditions, (ii) we can unused and the un-reacted component (iii) precipitants are not always needed and it easy to obtained composites (iv) it is possible to obtain highly pure synthesis product, (v) in this technique we can control the crystal size, morphology, composition, and polymorphism of the synthesized materials [73]. Table 1 below summarizes recent reports on chemical and hydrothermal synthesis techniques used to create Ag nanostructures of various shapes and sizes.

Table 1. Chemical and solvothermal synthesis technique of some silver nanostructures

Nanostructures	Method	Chemical used	Size	Year	References
Spherical	Chemical	Silver nitrate, Chloroauric acid, trisodium citrate dihydrate, Hydrochloric acid, Nitric acid	Diameter 48 nm	2010	[74]
	Chemical	Silver nitrate, Sodium citrate, Glycerol-water mixture	Diameter 20-100nm	2012	[75]
	Chemical	Silver nitrate, Trisodium citrate dihydrate, potassium iodide, sodium chloride, sodium bromide, sodium sulfide nonahydrate, anhydrous sodium carbonate, anhydrous sodium sulfate, trisodium phosphate dodecahydrate and ascorbic acid	Diameter 16-31nm	2014	[76]
	Chemical	Silver nitrate, trisodium citrate and tannic acid	Diameter 10-50nm	2014	[77]
	Chemical	Silver acetate, sodium borohydride, D-gluconic sodium salt and ferric chloride	Diameter 9.57 ± 2 nm	2018	[78]
Cubic	Chemical	Silver nitrate, Ammonia solution, n-hexadecyltrimethylammonium bromide	Edge length 55nm	2004	[79]
	Chemical	silver nitrate,ascorbic acid, cetyltrimethylammonium bromide, cetylpyridiniumchloride,potassium bromide ,Hydrochloric acid , Ammonium hydroxide solution (	Edge length 204±29nm	2015	[80]
	Chemical	Cetyltrimethylammonium chloride ascorbic acid, silver trifluoroacetate, iron(III) chloride, sodium borohydride, sodium chloride and 1,4-benzenedithiol	Edge length 36-56nm	2016	[81]
Nanoprism/ Nanoplate	Chemical	N,N-dimethylformamide, polymer poly(vinylpyrrolidone)	Edge length 80-200nm	2002	[82]
	Chemical	Silver nitrate, sodium borohydride, trisodium citrate and aqueous poly(sodium styrenesulphonate)	Edge length 20-65nm	2008	[83]
	Chemical	Silver nitrate, sodium borohydride, trisodium citrate, sodium hydroxide, nitric acid, sodium acetate, acetic acid, 1,10-phenanthroline, 2,4,5,7-tetrabromofluorescein	Edge length 100±20nm	2010	[84]
	Chemical	Silver nitrate, trisodium citrate, poly(vinylpyrrolidone), Hydrogen peroxide		2016	[85]
	Chemical	Silver nitrate, sodium borohydride, trisodium citrate, sodium hydroxide		2017	[86]
	Chemical	Trisodium Citrate, Hydrogen Peroxide, Silver Nitrate	Edge length 35-105nm	2017	[87]

Nanostructures	Method	Chemical used	Size	Year	References
	Solvothermal	Silver nitrate, poly(vinyl pyrrolidone), N,N-dimethylformamide	Edge length 50-150nm	2007	[88]
	Solvothermal	N,N-dimethylformamide , silver nitrate, poly (vinyl pyrrolidone)	Edge length few micrometer	2009	[89]
	Solvothermal	Silver nitrate, poly(vinyl pyrrolidone), N,N-dimethylformamide, Ferric chloride	Few micrometer	2011	[90]
Nanowire/nanorods	Chemical	Silver nitrate, CTAB, Ascorbic acid and Sodium hydroxide	Lenth 1-4 micrometer	2001	[91]
		Silver nitrate, sodium citrate and Sodium hydroxide	Up to 12micrometer length	2003	[92]
		Silver nitrate , Ascorbic acid and poly(methacrylic acid)	Few hundred micrometer	2004	[93]
		Silver nitrate, potassium tartaric, Silver nitrate, Sodium hydroxide	Length 1-10 micrometer	2006	[94]
		Potassium nitrate, Silver nitrate, Sodium borohydride	Average length ~535 nm and width ~131 nm	2017	[95]
		Silver nitrate, poly(vinyl pyrrolidone), sodium chloride and potassium bromide and ethanol	Length 20-50nm	2017	[96]
		Sodium tetrahydridoborate , hydrochloric acid, ascorbic acid, Cetyltrimethyl ammonium bromide , hexadecyltrimethyl ammonium chloride , Silver nitrate and tetrachloroaurate, Trisodium citrate	Length 150-800nm	2017	[97]
	Hydrothermal	Silver nitrate, Methenamine, 1,3-bis(cetyldimethylammonium) propane dibromide (16-3-16),	length ranging from several to tens of micrometers	2006	[98]
	Solvothermal	Silver nitrate , Poly(N-vinylpyrrolidone) ethylene glycol, and sodium sulfide (Na_2S)	length ranging from several to tens of micrometers	2010	[99]
	Solvothermal	Silver nitrate, poly(vinyl pyrrolidone), Ethylene glycol, Ferric chloride	Several micrometer	2011	[100]
Nanoflower	Chemical	Silver nitrate, rutin hydrate		2009	[101]
		Silver nitrate, Ascorbic acid and Poly(N-vinylpyrrolidone)		2009	[102]
		palmate-tuber salep, Silver nitrate,		2011	[103]
		Silver nitrate, Ammonium citrate dibasic, Aqueous ammonia solution, Boric acid, L-ascorbic		2017	[104]

3.1. Green Synthesis Growth Mechanism of Anisotropic Silver Nanostructures and The Role of The Reaction Parameters and Capping Agents

In the last century we have witnessed the enormous development of colloidal nanoparticle syntheses techniques [72] [102]. The growth mechanisms of these nanoparticles have been extensively studied due to their fundamental interest in theoretical and experimental

science. While colloidal nanoparticles exhibit enhanced electrical, magnetic, and chemical properties compared to bulk materials, these properties are highly dependent on size, shape, composition, and crystalline structure [105] [106]. So, the practical application of the colloidal particles in various field demands the alteration of the above properties. Thus, the principal knowledge on the growth of the nanoparticles provides the desired ability to manipulate the above parameters which results in the formation of the colloidal nanoparticles having preferred shape and sizes. Becker and Döring [107] were the first to develop classical theory for nucleation and growth of underlying processes of colloidal nanoparticles' syntheses and later it was improved by La Mer and co-workers in 1950 [108] and these models are still in use to explain the growth process of colloidal nanoparticles. There are two types of nucleation which occur in the colloidal synthesis process, those are homogeneous and heterogeneous nucleation [107] [108]. Homogeneous nucleation involves the uniform formation of nuclei within the bulk of the parent phase. In contrast, heterogeneous nucleation is facilitated by structural inhomogeneity, such as container surfaces, impurities, grain boundaries, and dislocations, which act as nucleation sites. Heterogeneous nucleation is significantly more favored in the liquid phase due to the readily available surfaces as stable nucleation sites. The Gibbs free energy change during nanoparticle surface formation provides insight into the thermodynamic driving force for nucleation. By considering a homogeneous nucleation process, the Gibbs free energy of spherical nanoparticles of radius r can be written as [107],

$$\Delta G_T = \frac{4}{3}\pi r^3 \Delta G_C + 4\pi r^2 \delta \tag{1}$$

Where, ΔG_C is the bulk crystal free energy, δ is the surface free energy. Now $\Delta G_C = -KT \ln(S) / V$ where, K is the Boltzmann constant and T is the temperature, S is the super saturation constant and V is the molar volume. As the crystal free energy is always negative and surface free energy is positive, a critical radius (r_c) must be reached so that particle remains stable in the solution without getting re-dissolve in the solution. The critical radius can be found out by setting $d\Delta G_T / dr$ to zero at $r = r_c$.

Which yields,

$$r_c = -2\delta/\Delta G_C = 2\delta v/2\ln(S) \tag{2}$$

Thus ΔG_T will pass through a critical value which can be written in terms of the critical radius as,

$$\Delta G_T^C = 4/3\pi r_c^3 \tag{3}$$

The rate of the nucleation (dn/dt) is related to the critical value of the total Gibbs free energy by the following relation as,

$$\frac{dn}{dt} = a \times \exp\left(-\Delta G_T^C / KT\right) \tag{4}$$

$$\frac{dn}{dt} = a \times \exp\left(-16\pi\delta^3 V^3 / 3K^3 T^3 \ln(S)\right) \tag{5}$$

Equation (5) clearly demonstrates that the nucleation rate is strongly influenced by several critical factors, including surface free energy, super saturation and temperature. Also, the effect of the super saturation on the nucleation rate is predominant as reported by other researchers. Capping agents significantly influence nanoparticle properties by modifying their surface free energy. This modification can lead to enhanced stability and in specific cases, induce anisotropic growth, resulting in particles with unique shapes. Temperature exerts a significant influence on nanoparticle synthesis, impacting both nucleation rates and the resulting particle morphology. By carefully controlling reaction temperature, it becomes possible to engineer nanoparticles with diverse and tailored shapes. So the reaction parameters can be tuned to get desired reaction rate and the synthesis of the nanoparticles of different size and shape are possible.

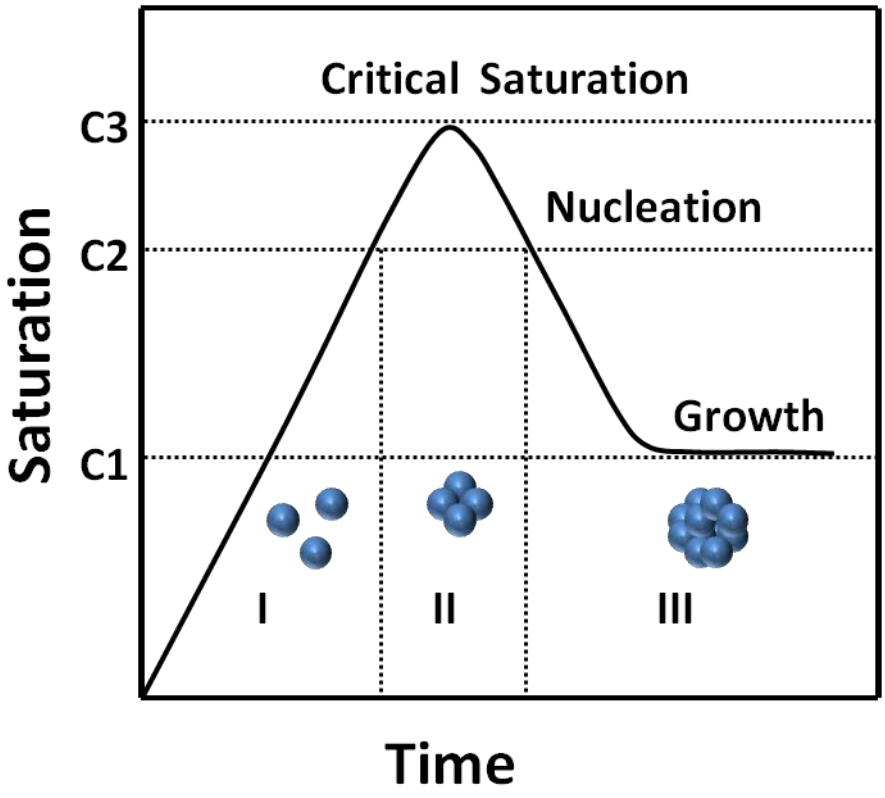

Figure 2. The La Mer diagram illustrates nanoparticle nucleation and growth. C1 represents the critical supersaturation for nucleation initiation, C2 indicates the onset of self-nucleation or burst nucleation, and C3 denotes the critical supersaturation level.

In contrast to homogeneous nucleation, heterogeneous nucleation preferentially occurs at specific sites within the material, such as phase boundaries or impurities [109]. These preferential sites are lower in surface energies therefore require less activation energies to promote particles growth. Consequently, heterogeneous nucleation is observed more commonly than homogeneous nucleation. Also, in seed mediate growth heterogeneous nucleation provides the driving force for the anisotropic growth process [110]. La Mer and his colleagues were the first to propose the concept of the burst nucleation and separate the two-process nucleation and growth [111]. Burst nucleation is characterized by a rapid and simultaneous formation of nuclei, followed by their immediate growth into particles without

further nucleation events. The mechanism of nucleation and growth can be explained in terms of the LaMer diagram as shown in the Fig. 2. In the region-I monomers are produced due the reduction of metal precursor and after certain time its concentration reaches at certain critical supersaturation level and homogeneous nucleation starts.

In region II, burst nucleation occurs when the saturation level overcomes the nucleation energy barrier, resulting in the rapid, simultaneous formation of many nuclei [111]. However, in region III, this rapid nucleation event significantly reduces the supersaturation level, effectively inhibiting further self-nucleation. Consequently, particle growth primarily proceeds through the diffusion of monomers from the solution to the existing particle surfaces.

Along with the La Mer mechanism of the nanoparticles nucleation and growth Ostwald ripening [112] and coalescence mechanism [113] are proven to be the suitable mechanism to describe the nanoparticles growth. Ostwald ripening [92] is the process by which larger particles grow at the expense of smaller particles in a system. This occurs because smaller particles, with their higher surface area-to-volume ratio, possess greater surface energy and are thus less stable. Consequently, they tend to dissolve more readily into the surrounding medium. The dissolved molecules then diffuse through the medium and attach to the surfaces of larger particles, causing them to grow. This ongoing process results in a reduction of the overall surface area, leading to a more thermodynamically stable system. In case of the Ostwald ripening nanoparticles with single domain will form [92] and in case of coalescence nanoparticles with multiple domains will form [93]. However, coalescence and orientated attachment [114] process are differing from each other due to the fact that in case of coalescence, there is no particular liking for the attachment in a certain crystallographic plane. But in case of the orientated attachment, growth [115] is taken place in continuous crystallographic planes. Application of the nanoparticles in the desired fields requires the synthesis of different shape and sizes as most of their physiochemical properties depends on the shape and sizes. Here surfactants can play a major role in synthesizing nanomaterials of different shape and sizes. Surfactants are preferentially attached to certain crystallographic plane at the nucleation sites by surface adsorption of surface-active molecules which determines the overall growth and the shape, size of the nanomaterials [115]. A diverse range of surfactants, encompassing ionic, nonionic, and amphoteric varieties, have been effectively employed to control the shape of synthesized nanomaterials. Polyvinylpyrrolidone (PVP), a nonionic polymer, is a prominent surfactant used for shape-controlled synthesis of metals, metal oxides, and metal chalcogenides with defined structures. PVP's versatility as a surfactant stems from its multiple functions, including shape control, surface stabilization, growth modification, nanoparticle dispersion, and reduction, depending on experimental conditions [116]. Surface free energy significantly influences nanocrystal morphology during crystal growth. In case metallic *fcc* structures the order of the surface free energy of the crystallographic planes is {111} < {110} < {100}. Due to the high surface energy of the {100} facets PVP attached preferentially [116] to it by direct binding through the oxygen atom and a Van der Waals type bonding is formed. In the synthesis of Ag nanostructures, multiply-twinned nanoparticles (MTPs) with dodecahedral geometry are frequently observed as the predominant seed morphology.

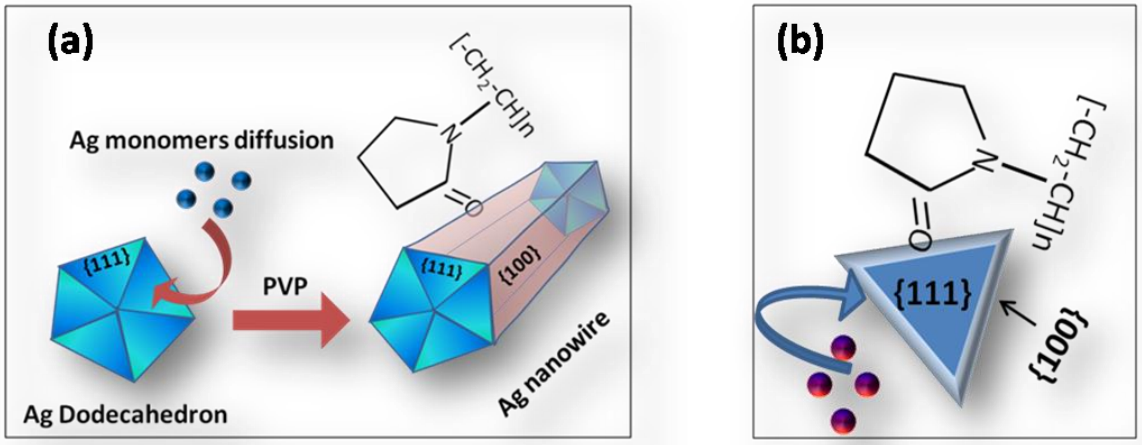

Scheme 1. (a) Schematic representation of the growth mechanism for Ag nanowire formation. (b) Schematic illustration of the growth mechanism of twinned nanostructures (TNS) in the presence of PVP.

Furthermore, their inherent twin defects contribute to their high reactivity. Thus, Ag monomers are attached to these high energy defects sites and leading to uniaxial growth. As decahedra grow into pentagonal nanorods, PVP preferentially attaches to the {100} side facets at the nanowire ends, rather than the {111} facets, as shown in Scheme 1(a) [116]. PVP passivates the nanorod side surfaces, while the ends remain active for Ag monomer attachment. This anisotropic growth results in rapid elongation of the nanorods into micrometer-long nanowires. On the other hand, in case of TNS {111} crystallographic facets present at both the top and bottom surfaces. The side facets of TNS contain twin planes of a {111} facet and a {100} facet with stacking faults [97].

As previously discussed, the surface energies of different facets in an fcc crystal structure exhibit a hierarchy. Side facets, typically composed of a combination of {111} and {100} planes, generally possess higher surface energies in compared to those of the top and bottom surfaces, which are predominantly {111} planes. Thus, newly formed Ag monomers produced in the solution by reduction get attached preferentially to the side facets and as a result lateral growth proceed extensively as shown in the Scheme 1(b). As the PVP get attached preferentially to the {111} facets the use of the PVP may hinder the uncontrolled growth of the TNS in larger nanoplate and results in the production of the TNS in the solution [117].

The diverse morphologies observed during synthesis likely arise from variations in the growth rates of crystallite faces, influenced by reaction temperature [118]. This differential growth is schematically illustrated in Scheme 2. The reduction of silver nitrate in the presence of seed particles (nanometer-sized) results in nanoparticles of varying sizes, formed through homogeneous and heterogeneous nucleation, and Ostwald ripening. Anisotropic structure formation, particularly during surfactant-assisted growth, is significantly influenced by the single, twinned, or multiple-plane arrangements found in the fcc structure of silver crystals. This process relies on two crucial factors: (i) dodecahedral multiply-twinned particles (MTPs) and (ii) PVP as a surfactant. TEM image analysis conducted during the initial stages of synthesis, as reported by Biswas et al. [16], confirms the presence of dodecahedral MTPs during early nucleation. These MTPs exhibit five-fold symmetry and are enclosed by ten {111} facets. Additionally, HRTEM imaging was used to determine the spacing between consecutive

{111} planes of the MTPs, which was measured to be 0.23 nm, aligning with values reported in the literature.

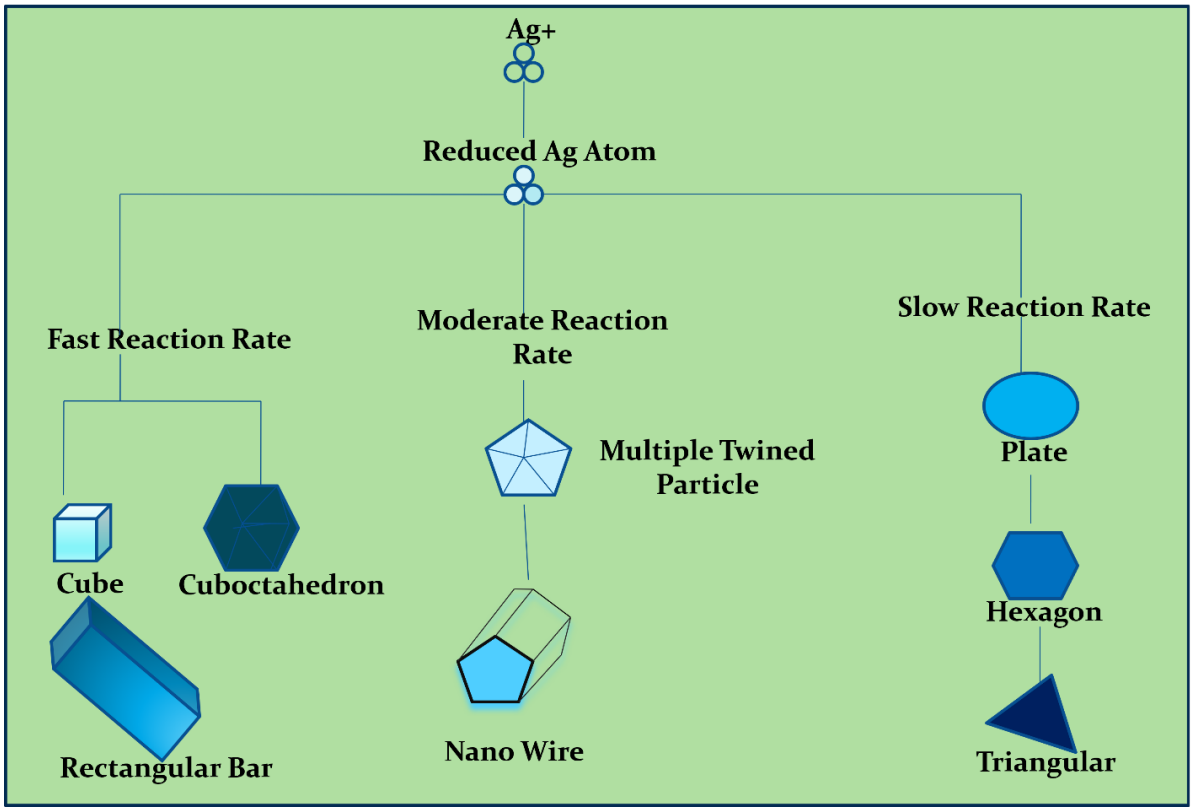

Scheme 2. A schematic depiction of evolution of shapes of different metal nanostructures starting from different seed crystals.

Scheme 2 schematically shows the evolution of silver nanostructures from seed crystals with Volterra disclinations [119]. Twin boundaries within multiply-twinned particles (MTPs) [120] represent high-energy sites, attracting silver atoms during Ostwald ripening and promoting uniaxial growth, leading to nanorod formation. The preferential binding of PVP to newly formed {100} side surfaces (through interactions with O or N2 units) inhibits lateral growth, while the exposed end surfaces remain reactive, facilitating continued growth along the longitudinal axis, resulting in nanowire structures. Previous studies [121] have shown that slight thermal fluctuations can induce structural changes in small nanoparticles. At smaller sizes, five-fold symmetric structures like icosahedra and decahedra exhibit greater stability, while cuboctahedral shapes become more stable at larger sizes. As particle size increases, structural fluctuations decrease, stabilizing the nanoparticle's morphology (single-crystalline or multi-twinned) and improving shape control. At lower temperatures, smaller silver seeds/nuclei experience greater structural fluctuations, allowing for the formation or removal of defects based on their energetic favorability [122] [123]. As the seed crystal grows, thermal energy becomes insufficient to alter the defect structure, locking it into a specific morphology. Consequently, lower-temperature synthesized samples exhibit higher defect densities, which can serve as preferential growth sites in the presence of PVP. Wiley et al. [122] showed that cubo-octahedral single crystals, small singly-twinned spheres, and decahedral multiply-twinned particles yield cubic crystals, spherical particles, five-fold twinned rods, and twinned wires, respectively.

4. Synthesis of anisotropic metal nanoparticles

4.1. One pot synthesis of different shaped silver anisotropic silver nanostructures

Biswas et al. [16] successfully synthesized Ag nanostructures with diverse morphologies using a facile one-pot chemical method. This approach involved varying the reaction temperature to control the final shape. In a typical synthesis, 7.5 mM AgNO3, 40 µM PVP, and 25 mM benzoic acid were simultaneously added to 30 mL of methanol. After 30 minutes of vigorous magnetic stirring at room temperature, a yellow-colored solution was obtained. The solution's temperature was then gradually raised from room temperature to 120 °C. Aliquots were collected at 10 °C intervals (60 °C, 70 °C, 80 °C, 90 °C, 100 °C, 110 °C, and 120 °C) and labeled as S-60, S-70, S-80, S-90, S-100, S-110, and S-120, respectively. The representatives of the TEM images for these samples are shown schematically in the accompanying Scheme 3 (for the original TEM images, please refer to Ref. 16).

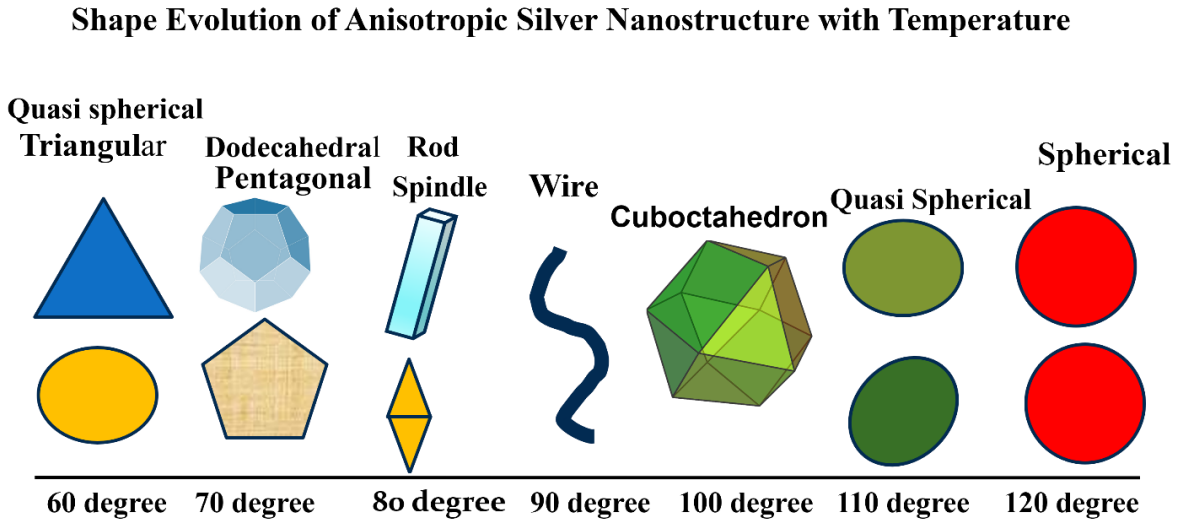

Scheme 3. A schematic depiction of different shaped silver nanoparticles those can be obtained at different stages of chemical synthesis (for the original images, please refer to Ref. 16).

4.2. Solvothermal synthesis technique to synthesize silver nanotriangle and silver nanoplates

There are number of earlier reports on syntheses of silver nanotriangle and silver nanoplates and amongst others, Biswas et al. [34] employed solvothermal synthesis approach for the production of triangular Ag nanostructures. In a standard experiment, 0.15 mM PVP was added to 40 mL DMF with continuous stirring, followed by 3 mM AgNO3. After 10 minutes of stirring, the mixture was transferred to an autoclave and heated to 160 °C. Samples were collected at 2, 4, and 8 hours, labeled as S1, S2, and S3, respectively. A schematic representation of the TEM images for these samples is provided in the accompanying Scheme 4 (for the original TEM images, please refer to Ref. 34).

Scheme 4. Schematic demonstration of triangular and plate like shapes of silver nanostructures synthesized at different temperatures (for the original images, please refer to Ref. 34).

4.2. Solvothermal synthesis technique to synthesize silver nanotriangle and silver nanoplates

Biswas et al. [12] reported the synthesis of gold nanostructures with diverse shapes using a seed-mediated approach, which involves a two-step process.

(i) Seed Preparation

Gold seeds (GNs) with a size distribution of 5-10 nm were prepared as follows: 10 mL of 0.2 M [reducing agent] was added to 10 mL of 0.05 mM HAuCl4 under vigorous magnetic stirring. The rapid addition of 1.2 mL ice-cold NaBH4 solution caused an immediate color change from yellow to brownish-yellow, indicating gold seed formation. The solution was stabilized for 2 hours before use.

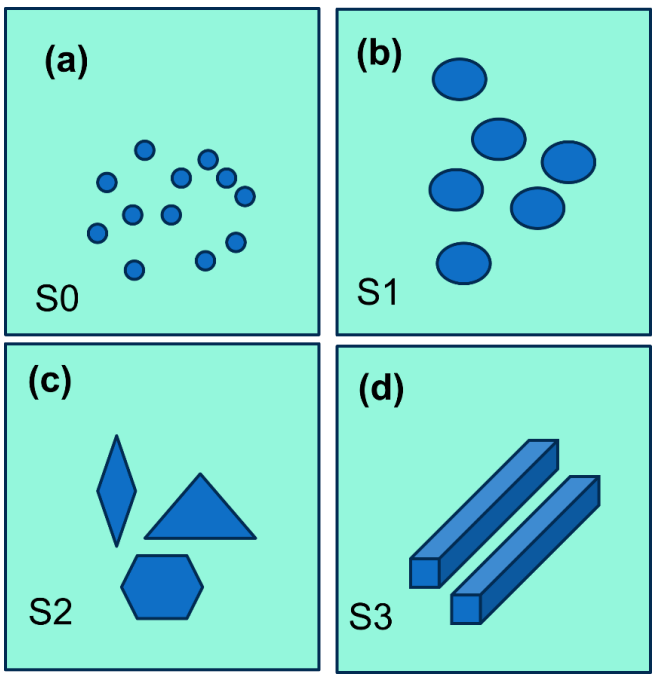

Scheme 5. The shapes of gold seeds (a) spherical gold nanoparticles (b) nano-rice (c), and gold nanorods (d) synthesized by seed mediated synthesis techniques are shown schematically (for the original images, please refer to Ref. 12).

(ii) Growth of Gold Nanostructures

50 mL of 0.2 M CTAB solution was prepared in four separate beakers. Subsequently, 0.5 mL, 1 mL, 1.5 mL, and 2 mL of 0.04 M AgNO3 were added to each beaker, respectively, and labeled as S1, S2, S3, and S4. 50 mL of 0.001 M HAuCl4 solution was then added to each beaker, followed by the gentle addition of 0.7 mL of 0.08 M ascorbic acid. Finally, 1.2 mL of the pre-prepared seed solution was added to each beaker, resulting in a distinct color change in each solution, indicating the formation of gold nanostructures with varying shapes and sizes. Schematic representations of the shapes of these samples are provided in the accompanying Scheme 5(a-d) (for the original TEM images, please refer to Ref. 12).

5. Surface Plasmons oscillation in metal nanoparticles: Influence of shape, sizes and environment

Metal nanoparticles exhibit remarkable plasmonic [124, 125] performance in the visible spectrum, with each metal displaying distinct optical properties. For instance, silver (Ag) nanoparticles exhibit minimal overlap between surface plasmon resonance (SPR) [124,125] and interband transitions [124,125], resulting in sharper and more intense plasmonic resonances compared to other metals like gold (Au) or copper (Cu). In contrast, Au nanoparticles show partial overlap between interband transitions and SPR, leading to broader resonance peaks [125] and reduced SPR intensity. The unique optical properties of metal nanostructures arise from the interaction between conduction band electrons and incident light. This interaction causes oscillatory motion of the loosely bound conduction electrons relative to the positively charged core, creating electric dipoles due to charge separation. Coulombic forces between these dipoles act as a restoring force, sustaining the oscillation. The energy of this oscillatory motion is quantized as plasmons [126]. Scheme 6 schematically depicts localized surface plasmon resonance (LSPR) in metal nanostructures under an external electromagnetic field.

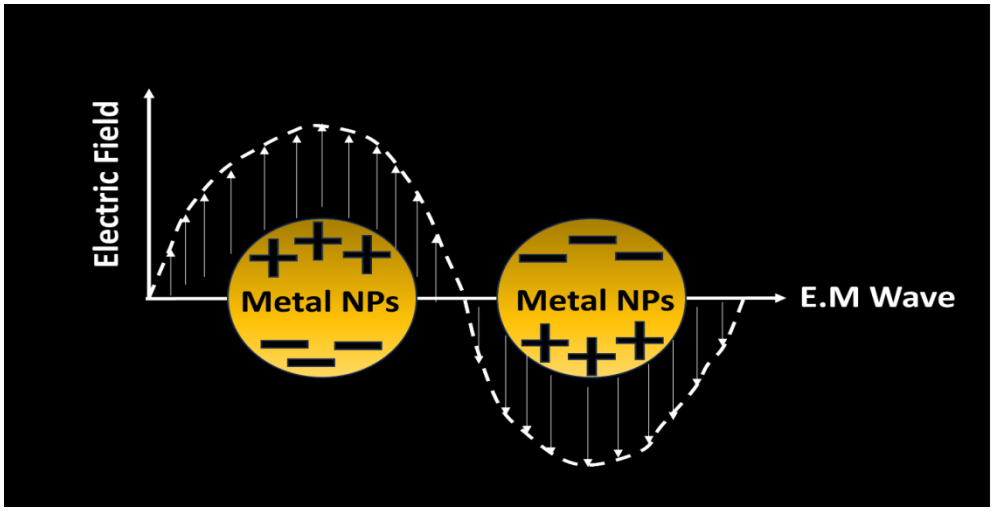

Scheme 6. A schematic of the localized SPR in metal nanostructures.

The theoretical foundation of localized surface plasmon resonance (LSPR) was established by G. Mie [127] in the early 20th century. An exact solution to Maxwell's equations were reported to describe the interaction of light with an isotropic spherical nanoparticle embedded in a non-absorbing, homogeneous medium. This work extensively examines how nanoparticle size, shape, and surrounding medium dielectric properties affect optical properties. Under the quasi-static approximation, where particle size is much smaller than the incident light wavelength, the electric field is assumed uniform across the nanoparticle's surface. This approximation simplifies the analysis while still capturing the essential features of LSPR.

The molecular polarizability (α) of spherical metal nanoparticles embedded in a medium with dielectric constant (εm), assuming the quasi-static approximation holds, can be described as,

$$\alpha = 3V\varepsilon_0\left(\varepsilon - \varepsilon_m / \varepsilon + 2\varepsilon_m\right) \tag{6}$$

Where $V = 4/3\pi a^3$ is the volume of the nanoparticles and a is the radius. Now the dielectric function $\varepsilon = \varepsilon_1 + i\varepsilon_2$, where ε_1 and ε_2 real and imaginary parts constitute the dielectric function. However, for noble metals, the imaginary part exhibits minimal dependence on the incident wave's frequency. Consequently, the real part of the dielectric function primarily governs its behavior. A significant resonance phenomenon occurs at the Surface Plasmon Resonance (SPR) frequency, characterized by the condition: $\varepsilon_1 + 2\ \varepsilon_m = 0$, where ε_1 denotes the real component of the metal's dielectric function, and ε_m represents the dielectric constant of the surrounding medium. At the resonant frequency of the surface plasmon, the nanoparticle's polarizability exhibits a maximum. The extinction and scattering efficiencies of these nanoparticles can be quantitatively described in terms of their dipolar polarizability,

$$E_{ext} = \left(\frac{8\pi^2 a^3 \varepsilon_m^{1/2}}{\lambda}\right) \mathrm{Im}\left(\frac{\varepsilon - \varepsilon_m}{\varepsilon + 2\varepsilon_m}\right) \tag{7}$$

$$E_{scatt} = \left(\frac{128\pi^4 a^4 \varepsilon_m^2}{\lambda^4}\right)\left(\frac{\varepsilon - \varepsilon_m}{\varepsilon + 2\varepsilon_m}\right) \tag{8}$$

For larger particle sizes, higher-order multipoles, particularly the quadrupole term, become crucial for accurately calculating the extinction and scattering spectra. Extending the quasi-static approximation allows for the mathematical expression of extinction and scattering efficiencies.

$$E_{ext} = \left(\frac{8\pi\ a\ \varepsilon_m^{1/2}}{\lambda}\right) \mathrm{Im}\left[\left(\frac{\varepsilon - \varepsilon_m}{\varepsilon + 2\varepsilon_m}\right) + \left(\frac{\pi^2 a^2 \varepsilon_m}{3\lambda^2}\right)\left(\frac{\varepsilon - \varepsilon_m}{\varepsilon + 1.5\varepsilon_m}\right) + \left(\frac{2\pi a \varepsilon_m}{15\lambda^2}\right)(\varepsilon - 1)\right] \tag{9}$$

$$E_{scatt} = \left(\frac{128\pi^4 a^4 \varepsilon_m^2}{3\lambda^4}\right)\left[\left(\frac{\varepsilon - \varepsilon_m}{\varepsilon + 2\varepsilon_m}\right)^2 + \left(\frac{2\pi^4 a^4 \varepsilon_m^2}{15\lambda^2}\right)\left(\frac{\varepsilon - \varepsilon_m}{\varepsilon + 1.5\varepsilon_m}\right)^2 + \left(\frac{4\pi^4 a^4 \varepsilon_m^2}{225\lambda^2}\right)(\varepsilon - 1)\right] \tag{10}$$

In bulk metals, the dielectric function is influenced by two types of transitions: interband transitions, which involve electronic transitions between states within the same band, and intraband transitions, which occur between different bands. Interband transitions pertain to bound electrons, while intraband transitions involve the movement of free electrons. The Drude model [125] provides a framework for describing the dynamics of free electrons. The equation of motion for an electron (mass '*m*') within an external electromagnetic field (frequency '*ν*') is defined by the following model,

$$m\frac{d^2x}{dt}+\gamma_0\frac{dx}{dt}+Kx=eE_0e^{-i\nu t} \tag{11}$$

In this context, where γ_0 represents the bulk damping constant, *e* denotes the electronic charge, and *K* signifies the force constant (which reduces to zero for bulk metals within the free electron model), the solution to Equation (11) assumes the following form,

$$x=\frac{eEe^{-i\nu t}}{m\left(i\gamma_o\nu+\nu^2\right)} \tag{12}$$

If the electron volume concentration is *N*, then the polarizability per unit volume can be expressed as,

$$P=Nex=\frac{Ne^2E_0e^{-i\nu t}}{m\left(i\gamma_0\nu+\nu^2\right)} \tag{13}$$

Using the Equation (13) the ε can be extracted from the relation $P = (\varepsilon_{intra}+1)\,\varepsilon_0 E$ and can be expressed in simplified form,

$$\varepsilon_{intra}=1-\frac{\nu_p^2}{\left(\nu^2+i\gamma_0\nu\right)} \tag{14}$$

Where, υ_p is the bulk Plasmon frequency. As we have discussed earlier, $\varepsilon = \varepsilon_1+i\,\varepsilon_2$, the real and imaginary components of the dielectric function, ε, can be derived from Equation (14) and are expressed as follows,

$$\varepsilon_1=1-\frac{\nu_p^2}{\left(\nu^2+\gamma_0^2\right)},\ \varepsilon_2=\frac{\nu_p^2\gamma_0}{\left(\nu^3+\gamma_0^2\nu\right)} \tag{15}$$

In terms of the expression of the real part of the dielectric function given by Equation (15) the resonant condition $\varepsilon_1+2\varepsilon_m = 0$ can now be modified as,

$$1-\frac{\nu_p^2}{\left(\nu_{SPR}^2+\gamma_0^2\right)}+2\varepsilon_m=0 \tag{16}$$

At high frequency $\upsilon^2>>\gamma_0^2$ and from Equation (16) we can obtain the expression for the SPR frequency which is given by,

$$\nu_{SPR} = \frac{\nu_p}{(1+2\varepsilon_m)^{1/2}} \tag{17}$$

The SPR frequency described by Equation (17) does not align with experimental results, as it fails to account for the contribution of bound electrons. The presence of bound electrons establishes a positive background charge, effectively screening the free electrons and consequently diminishing the bulk plasma frequency, υ_{SPR}. For instance, the bulk plasma frequency of silver (Ag), as predicted by the Drude model, corresponds to an energy value of approximately 9.2 eV. However, experimental measurements reveal a bulk plasma frequency of 3.9 eV for silver (Ag), which deviates significantly from the Drude model's prediction. To accurately describe the dielectric behavior of nanoparticles, the influence of bound electrons must be incorporated. Consequently, the dielectric function can be reformulated as described in [126].

$$\varepsilon_{total} = \varepsilon_{inter} + \varepsilon_{intra} \ \textbf{or}, \ \varepsilon_{total} = \varepsilon_{\text{int } er} + 1 - \frac{\nu_p^2}{(\nu^2 + i\gamma\nu)} \tag{18}$$

Here, γ, the surface damping term, is related to the bulk damping constant by,

$$\gamma = \gamma_0 + V_F/R \tag{19}$$

Where, V_F is the Fermi velocity at the metal surface and R is the radius. The far-field spectral characteristics of spherical nanoparticles in an external electric field are rigorously derived within Mie theory by analytically solving Maxwell's equations via spherical harmonic series expansion. A spectrum of plasmonic modes, starting with fundamental dipolar modes and extending to higher-order multipolar modes, is encompassed by this analytical solution [128]. While Mie theory provides a robust framework for analyzing the optical properties of solid, spherical metal nanoparticles, its applicability extends beyond this specific geometry. The theory can be adapted to encompass systems exhibiting spherical symmetry, such as core-shell nanoparticles. It is well-established that the shape and dimensions of nanoparticles exert a profound influence on their observed optical properties. To address the optical behavior of anisotropic particles, such as oblate and ellipsoidal nanoparticles, Mie theory has been extended under the purview of the dipolar approximation, resulting in the formulation of Gans theory [128]. Gans theory has demonstrated remarkable efficacy in elucidating the observed plasmonic scattering and absorption phenomena in nanorods, effectively treating them as a specialized case of ellipsoidal nanoparticles. Gans theory provides detailed mathematical expressions for the scattering and absorption cross-sections of ellipsoidal nanoparticles [129, 130].

The environment where the nanoparticles are embedded has also significant effect on its optical properties. The real component of the dielectric function is expressed as,

$$\varepsilon_1 = 1 - \frac{\nu_p^2}{(\nu^2 + \gamma_0^2)} \tag{20}$$

In the visible and infrared region $\gamma_0 << \upsilon_{p,}$ Equation (28) is reduced to $\varepsilon_1 = 1-\upsilon_p^2/\upsilon^2$. Now when the resonance occurs, $\varepsilon_1 = -2\varepsilon_m$ and then $\upsilon = \upsilon_{SPR}$. Hence, under resonant conditions, we can formulate,

$$\nu_{SPR} = \frac{\nu_p}{(1+2\varepsilon_m)^{1/2}}. \tag{21}$$

In terms of the wavelength, the Equation (21) has been reduced to [131],

$$\lambda_{SPR} = \lambda_P(1+2\varepsilon_m)^{1/2} = \lambda_p(1+2n_m^2)^{1/2} \tag{22}$$

Where, $\varepsilon_m = n_m^2$ and n_m is the refractive index of the medium. Equation (22) shows that increasing refractive index shifts the LSPR peak to longer wavelengths. It is also evident from the simulated curve obtained from the relation presented in Equation (22) that the variation of the peak position with the refractive index is almost linear. This relationship serves as the foundation for high-sensitivity detection of changes in the refractive index (R.I.) or molecular-level variations, making it a viable platform for LSPR-based sensing. Additionally, the intensity and peak position of the SPR band are influenced by temperature. Previous studies have shown that as temperature increases, the SPR band broadens [132], resulting in a drop in intensity and a red shift in the SPR peak position. Electron–phonon scattering, nanoparticle thermal expansion, and temperature-dependent medium permittivity explain this behavior. Considering electron scattering at the nanoparticle surface, Equation (16) can be modified as [133],

$$\nu_{SPR} = \left[\frac{\nu_p^2}{(1+2\varepsilon_m+\varepsilon_{\text{int }er})} - \gamma^2\right]^{1/2} \tag{23}$$

Where, $\gamma = \gamma_0 + V_F/R$. As the surface temperature of metal nanoparticles rises, the particle radius expands, leading to a decrease in the damping factor (γ). This reduction in γ decreases the overall SPR energy, leading to a broadening of the SPR band and a reduction in its intensity. Additionally, the SPR peak experiences a slight blue shift. Studies have shown that the decrease in SPR peak intensity and the shift in its position with increasing temperature are almost linear. These temperature-dependent properties of nanoparticles are effectively utilized in temperature sensing applications, both in research and industry.

7. Conclusions

Here in this review, we have presented an outline of the synthesis methods utilized to create anisotropic nanoparticles with regulated sizes, shapes, and compositions with particular attention to the syntheses and Plasmonic properties of Ag and Au. The effectiveness, repeatability, and scalability of several techniques, such as chemical reduction, seed-mediated development, and template-assisted approaches are examined. Understanding how surfactants, reducing agents, and reaction conditions contribute to anisotropic development is emphasized. Recent developments in green synthesis techniques also demonstrate the trend toward eco-friendly practices. The review sheds light on how exact control over the anisotropy of

nanoparticles improves their functional characteristics and permits their intended uses in photonics, biomedicine, and catalysis. The results highlight how these methods could help develop the creation of next-generation anisotropic nanomaterials. We explored the theoretical principles of surface plasmon resonance in metal nanostructures and discussed how the aspect ratio of anisotropic nanoparticles affects their localized surface plasmon resonance properties. This understanding will guide the design and tuning of metal nanoparticle's shape and size for specific applications, ranging from sensing to lasing.

Multidisciplinary Domains

This research covers the domains: (a) Material Science, and (b) Environment.

Funding

No funding to declare.

Acknowledgement

We are thankful to MoE, NIT Durgapur for the necessary support. Also thankful to the reviewer for constructive comments. We thank Dr. R. Biswas for the Invitation.

Conflicts of Interest

There is no conflicts of interest to declare.

Declaration on AI Usage

The authors declare that the article has been prepared without the use of AI tools.

References

[1] Xia, Y.; Chen, Q.; Banin, U. Introduction: Anisotropic Nanomaterials, ACS Publication: Chem. Rev., USA, **2023**, pp. 3325–3328, https://doi.org/10.1021/acs.chemrev.3c00092

[2] Burrows, N. D. *et al.* Anisotropic Nanoparticles and Anisotropic Surface Chemistry. *J. Phys. Chem. Lett.* **2016**, 7, 4, 632–641, https://doi.org/10.1021/acs.jpclett.5b02205

[3] Wei, M.; Deng, T.; Zhang, Q.; Cheng, Z.; Li, S. Seed-Mediated Synthesis of Gold Nanorods at Low Concentrations of CTAB, *ACS Omega* **2021**, 6, 13, 9188–9195, https://doi.org/10.1021/acsomega.1c00510

[4] Scarabelli, L.; Liz-Marzán, L. M. An Extended Protocol for the Synthesis of Monodisperse Gold Nanotriangles, *ACS Nano* **2021**, 15, 12, 18600–18607, https://doi.org/10.1021/acsnano.1c10538

[5] Liebig, F. *et al.* A simple one-step procedure to synthesise gold nanostars in concentrated aqueous surfactant solutions, *RSC Adv*. **2019**, 9, 23633-23641, https://doi.org/10.1039/C9RA02384D

[6] Das, A. K.; Kalita, J. J.; Borah, M. *et al.* Papaya latex mediated synthesis of prism shaped proteolytic gold nanozymes. *Sci Rep*, **2023**,13, 5965-5978. https://doi.org/10.1038/s41598-023-32409-7

[7] Singh, K. Rb,; Natarajan, A.; Pandey, S. S.; Bioinspired Multifunctional Silver Nanoparticles for Optical Sensing Applications: A Sustainable Approach, *ACS Appl. Bio Mater.* **2023**, 6, 11, 4549–4571, https:// DOI: 10.1021/acsabm.3c00669

[8] Hartland, G. V.; Besteiro, L. V.; Johns, P.; Govorov, A. O. What's so Hot about Electrons in Metal Nanoparticles? *ACS Energy Lett.* **2017**, 2, 7, 1641–1653, https://doi.org/10.1021/acsenergylett.7b00333

[9] Zhou, Y.; Jin, C.; Li, Y.; Shen, W. Dynamic behavior of metal nanoparticles for catalysis, *Nanotoday*, **2018**, 20, 101-120, https://doi.org/10.1016/j.nantod.2018.04.005

[10] Klębowski, B.; Depciuch, J.; Parlińska-Wojtan, M.; Baran, J. Applications of Noble Metal-Based Nanoparticles in Medicine, *Int. J. Mol. Sci*. **2018**,19, 4031, http://doi: 10.3390/ijms19124031

[11] Si, P. *et al.*, Gold nanomaterials for optical biosensing and bioimaging, *Nanoscale Adv*., **2021**, 3, 2679–2698. https://doi.org/10.1039/D0NA00961J

[12] Biswas, S.; Chakraborty, J.; Agarwal, A,; Kumbhakar, P. Gold nanostructures for the sensing of pH using a smartphone, *RSC Adv*. **2019**, 9, 34144-34151, https://doi.org/10.1039/C9RA07101F

[13] Krishna, P. G. *et al.*, Photocatalytic Activity Induced by Metal Nanoparticles Synthesized by Sustainable Approaches: A Comprehensive Review, *Front. Chem*. **2022**, 10, 917831, https://doi.org/10.3389/fchem.2022.917831

[14] Jana, J.; Ganguly, M,; Pal, T, Enlightening surface plasmon resonance effect of metal nanoparticles for practical spectroscopic application, *RSC Adv*., **2016**, 6, 86174-86211, https://doi.org/10.1039/C6RA14173K

[15] Semchuk, O. Yu.; Biliuk, A. A.; Havryliuk, O. O.; Biliuk, A. I. Kinetic theory of electroconductivity of metal nanoparticles in the condition of surface plasmon resonance, *Appl. Surf. Sci. Adv*., **2021**,3, 100057, https://doi.org/10.1016/j.apsadv.2021.100057

[16] Biswas, S.; Kole, A. K.; Sarkar, R.; Kumbhakar, P. Synthesis of anisotropic nanostructures of silver for its possible applications in glucose and temperature sensing, *Mater. Res.*, **2014**, 1, 045043, https://DOI 10.1088/2053-1591/1/4/045043

[17] López-Lozano, X.; Barron, H.; Mottet, C.; Weissker, H. Aspect-ratio- and size-dependent emergence of the surface-plasmon resonance in gold nanorods – an ab initio TDDFT study, *Phys. Chem. Chem. Phys*. **2014**,16, 1820-1823, https://doi.org/10.1039/C3CP53702A

[18] Chapagain, P. *et al.*, Tuning the Surface Plasmon Resonance of Gold Dumbbell Nanorods, *ACS Omega*, **2021**, 6, 10, 6871–6880, https://doi.org/10.1021/acsomega.0c06062

[19] Yu, S. *et al.*, Noble Metal Nanoparticle-Based Photothermal Therapy: Development and Application in Effective Cancer Therapy, *Int. J. Mol. Sci*., **2024**, 25, 5632, https://doi.org/10.3390/ijms25115632

[20] Kenmotsu, S. *et al.*, Surface-Enhanced Raman Scattering on Size-Classified Silver Nanoparticles Generated by Laser Ablation, *ACS Omega*, **2024**, 9, 36, 37716–37723, https://doi.org/10.1021/acsomega.4c03046

[21] Estrada-Mendoza, T. A., Willett, D, Chumanov, G. Light Absorption and Scattering by Silver/Silver Sulfide Hybrid Nanoparticles, *J. Phys. Chem. C* **2020**, 124, 49, 27024–27031,https:// DOI:10.1021/acs.jpcc.0c08247

[22] Burrows, N. D. *et al.*, Anisotropic Nanoparticles and Anisotropic Surface Chemistry, *J. Phys. Chem. Lett*., **2016**, 7, 4, 632–641, https://DOI: 10.1021/acs.jpclett.5b02205

[23] Pozzi, M. *et al.*, Visualization of the High Surface-to-Volume Ratio of Nanomaterials and Its Consequences, *J. Chem. Educ*. **2024**, 101, 8, 3146–3155, https://doi.org/10.1021/acs.jchemed.4c00089

[24] van Etten, M. P. C., Zijlstra, B., Hensen, E. J. M., Filot, I. A. W., Enumerating Active Sites on Metal Nanoparticles: Understanding the Size Dependence of Cobalt Particles for CO Dissociation, *ACS Catal.*, **2021**, 11, 14, 8484–8492, https://doi.org/10.1021/acscatal.1c00651

[25] Xu, J.; Zhang, W.; Guo, Y.; Chen, X.; Zhang, Y. Metal nanoparticles as a promising technology in targeted cancer treatment, *Drug Deliv*., **2022**, 29, 664–678, https:// doi: 10.1080/10717544.2022.2039804

[26] Maturi, M. *et al.*, Surface-Stabilization of Ultrathin Gold Nanowires for Capacitive Sensors in Flexible Electronics, *ACS Appl. Nano Mater.*, **2021**, 4, 9, 8668–8673, https://doi.org/10.1021/acsanm.1c01849

[27] Vargas, J. A. *et al.*, Ultrathin Gold Nanowires with the Polytetrahedral Structure of Bulk Manganese, *ACS Nano* **2018,** 12, 9, 9521–9531, https:// DOI: 10.1021/acsnano.8b05036

[28] Das, R. *et al.*, Tunable High Aspect Ratio Iron Oxide Nanorods for Enhanced Hyperthermia, *J. Phys. Chem. C*, **2016**, 120, 18, 10086–10093, https://doi.org/10.1021/acs.jpcc.6b02006

[29] Bushra, R. *et al.*, Recent advances in magnetic nanoparticles: Key applications, environmental insights, and future strategies, *SM&T*, **2024**, 40, 00985, https: DOI:10.1016/j.susmat.2024.e00985

[30] Chang, D. *et al.*, Biologically Targeted Magnetic Hyperthermia: Potential and Limitations, *Front Pharmacol*., **2018**, 9, 831, https://doi.org/10.3389/fphar.2018.00831

[31] Nair, A. S.; Peining, Z.; Babu, V. J.; Shengyuan, Y.; Ramakrishn, S. Anisotropic TiO2 nanomaterials in dye-sensitized solar cells, *Phys. Chem. Chem. Phys*., **2011**,13, 21248-21261, https://doi.org/10.1039/C1CP23085A

[32] Kwon, H.; Yang, Y.; Kim, G.; Gima, D.; Ha, M. Anisotropy in magnetic materials for sensors and actuators in soft robotic systems, *Nanoscale*, **2024**,16, 6778-6819, https://doi.org/10.1039/D3NR05737B

[33] Hu, J,; Brackemyer, C. A.; Byun, H.; Kim, J. Enhanced Stability of Anisotropic Gold Nanoparticles by Poly(N-isopropylacrylamide), *J. Mater. Sci. Technol.*, **2014**, 30, 5, 441-448, https://doi.org/10.1016/j.jmst.2014.03.012

[34] Biswas, S., Kole, A. K., Tiwary, C. S., Kumbhakar, P., Observation of Size-Dependent Electron–Phonon Scattering and Temperature-Dependent Photoluminescence Quenching in Triangular-Shaped Silver Nanoparticles, *Plasmonics*, **2016**, 11, 593–600, https: DOI:10.1007/s11468-015-0072-6

[35] Mao, Qi. *et al.*, A novel passive detection method for glucose sensing based on enzyme-catalyzed reaction regulating magnetic anisotropy, *Chem. Eng. J*., **2022**, 446, 136844, https://doi.org/10.1016/j.cej.2022.136844

[36] Kohout, C.; Santi, C.; Polito, L., Anisotropic Gold Nanoparticles in Biomedical Applications, *Int. J. Mol. Sci*., **2018**, 19, 3385, https:// DOI: 10.3390/ijms19113385

[37] Gayathri, R. *et al.*, Plasmonic random laser enabled artefact-free wide-field fluorescence bioimaging: uncovering finer cellular features, *Nanoscale Adv*., **2022**,4, 2278-2287, https://doi.org/10.1039/D1NA00866H

[38] Kavalaraki, A., Spyratou, E., Kouri, M. A.; Efstathopoulos, E. P., Gold Nanoparticles as Contrast Agents in Ophthalmic Imaging, *Optics*, **2023**, 4, 74-99, https://doi.org/10.3390/opt4010007

[39] Yingxin, W.; Qianqian, Z. Preparation of novel anisotropic gold nanoplatform as NIR absorbing agents for photothermal therapy of liver cancer and enhanced ultrasound contrast imaging, *Mater. Res. Express*, **2020**, 7, 125006, https:// DOI 10.1088/2053-1591/abd0a7

[40] Chang, F.; Davies, G. From 0D to 2D: Synthesis and bio-application of anisotropic magnetic iron oxide nanomaterials, *Progress in Materials Science*, **2024**, 144, 101267, https://doi.org/10.1016/j.pmatsci.2024.101267

[41] Das, A.; Yadav, N.; Manchala, S.; Bungla, M.; Ganguli, A. K. Mechanistic Investigations of Growth of Anisotropic Nanostructures in Reverse Micelles, *ACS Omega* **2021**, 6, 2, 1007–1029, https://doi.org/10.1021/acsomega.0c04033

[42] Kiani, F.; Tagliabue, G. High Aspect Ratio Au Microflakes via Gap-Assisted Synthesis, *Chem. Mater*. **2022**, 34, 3, 1278–1288, https://doi.org/10.1021/acs.chemmater.1c03908

[43] Sajanlal, P. R.; Sreeprasad, T. S.; Samal, A. K.; Pradeep, T. Anisotropic nanomaterials: structure, growth, assembly, and functions, *Nano Rev*., **2011**, 2, 5883, https:// doi: 10.3402/nano.v2i0.5883

[44] Xia, Y.; Gilroy, K. D.; Peng, H.; Xia, X. Seed-Mediated Growth of Colloidal Metal Nanocrystals, *Angew. Chem*., **2017**, 56, 60-95, https://doi.org/10.1002/anie.201604731

[45] Yamamoto, E.; Kurimoto, D.; Ito, K.; Hayashi, K.; Kobayashi, M.; Osada, M. Solid-state surfactant templating for controlled synthesis of amorphous 2D oxide/oxyhydroxide nanosheets, *Nat. Commun*., **2024**, 15, 6612, https://doi.org/10.1038/s41467-024-51040-2

[46] Thanh, N. T. K.; Maclean, N.; Mahiddine, S. Mechanisms of Nucleation and Growth of Nanoparticles in Solution, *Chem. Rev*., **2014**, 114, 15, 7610–7630, https://doi.org/10.1021/cr400544s

[47] Papanikolaou, G.; Centi, G.; Perathoner, S.; Lanzafame, P. Green synthesis and sustainable processing routes, *Curr. Opin. Green Sustain. Chem*., **2024**, 47, 100918, https://doi.org/10.1016/j.cogsc.2024.100918

[48] Baig, N.; Kammakakam, I.; Falath, W. Nanomaterials: a review of synthesis methods, properties, recent progress, and challenges, *Mater. Adv.*, **2021**, 2, 1821-1871, https://doi.org/10.1039/D0MA00807A

[49] Ijaz, I.; Gilani, E.; Nazir, A.; Bukhari, A. Detail review on chemical, physical and green synthesis, classification, characterizations and applications of nanoparticles, Green *Chemistry Letters and Reviews*, **2020**, 13(3), 223–245, https://doi.org/10.1080/17518253.2020.1802517

[50] El-Eskandarany, M. S.; Al-Hazza, A.; Al-Hajji, L. A.; Ali, N.; Al-Duweesh, A. A.; Banyan, M.; Al-Ajmi, F. Mechanical Milling: A Superior Nanotechnological Tool for Fabrication of Nanocrystalline and Nanocomposite Materials, *Nanomaterials (Basel)*, **2021**, 11, 2484, https://doi.org/10.3390/nano11102484

[51] Ali, M.; Abdala, A. Large scale synthesis of hexagonal boron nitride nanosheets and their use in thermally conductive polyethylene nanocomposites, International Journal of Energy Research, *Int J Energy Res*., **2021**, 1–14, https://doi.org/10.1002/er.7149

[52] Pramanik, A. *et al.*, Synthesis of bilayer graphene nanosheets by pulsed laser ablation in liquid and observation of its tunable nonlinearity, *Appl. Surf. Sci.*, **2020**, 499, 143902, https://DOI:10.1016/j.apsusc.2019.143902

[53] Tseng, A. A.; Chen, K.; Chen, C. D.; Ma, K. J. Electron beam lithography in nanoscale fabrication: recent development, *IEEE. T. COMP. PACK. MAN.*, **2003**, 26, 141-149, https:// DOI:10.1109/TEPM.2003.817714

[54] Barad, H.; Kwon, H.; Alarcón-Correa, M.; Fischer, P. Large Area Patterning of Nanoparticles and Nanostructures: Current Status and Future Prospects, *ACS Nano* **2021**, 15, 4, 5861–5875, https://doi.org/10.1021/acsnano.0c09999

[55] Han, H.; Huang, Z; Lee, W. Metal-assisted chemical etching of silicon and nanotechnology applications, *Nanotoday*, **2014**, 9, 271-304, https://doi.org/10.1016/j.nantod.2014.04.013

[56] Wendisch, F. J.; Rey, M.; Vogel, N.; Bourret, G. R. Large-Scale Synthesis of Highly Uniform Silicon Nanowire Arrays Using Metal-Assisted Chemical Etching, *Chem. Mater*. **2020**, 32, 21, 9425–9434, https:// DOI: 10.1021/acs.chemmater.0c03593

[57] Kumar, S.; Bhushan, P.; Bhattacharya, S., Fabrication of Nanostructures with Bottom-up Approach and Their Utility in Diagnostics, Therapeutics, and Others, Environmental, *Chemical and Medical Sensors*. **2017**,167–198, https://doi: 10.1007/978-981-10-7751-7_8

[58] Baig, N.; Kammakakam, I.; Falatha, W. Nanomaterials: a review of synthesis methods, properties, recent progress, and challenges, *Mater. Adv.*, **2021**, 2, 1821-1871, https://doi.org/10.1039/D0MA00807A

[59] Biswas, S.; Kole, A. K.; Kumbhakar, P. Observation of two-photon induced three-photon absorption in chemically synthesized silver nanostructures, *Chem. Phys. Lett*., **2015**, 629, 70-75, https:// DOI:10.1016/j.cplett.2015.04.021

[60] Sun, Y.; Xia, Y. Shape-Controlled Synthesis of Gold and Silver Nanoparticles, *Science*, **2002**, 298, 2176-2179, https;// DOI: 10.1126/science.1077229

[61] Danks, A. E.; Hall, S. R.; Schnepp, Z. The evolution of 'sol–gel' chemistry as a technique for materials synthesis, *Mater. Horiz*., **2016**, 3, 91-112, https://doi.org/10.1039/C5MH00260E

[62] Bokov, D. *et al.*, Nanomaterial by Sol-Gel Method: Synthesis and Application, *Adv. Mater. Sci. Eng*., 2021, 2021, 1-21, https://doi.org/10.1155/2021/5102014

[63] Jenkins, J. A.; Wax, T. J.; Zhao, J. Seed-Mediated Synthesis of Gold Nanoparticles of Controlled Sizes to Demonstrate the Impact of Size on Optical Properties, *J. Chem. Educ.*, **2017**, 94, 8, 1090–1093, https://DOI:10.1021/acs.jchemed.6b00941

[64] Walker, N. *et al.*, Extracting structured seed-mediated gold nanorod growth procedures from scientific text with LLMs, *Digital Discovery*, **2023**, 2, 1768-1782, https://doi.org/10.1039/D3DD00019B

[65] Biswas, S.; Kole, A. K.; Tiwary, C. S.; Kumbhakar, P. Enhanced nonlinear optical properties of graphene oxide–silver nanocomposites measured by Z-scan technique, *RSC Adv*., **2016**, 6, 10319-10325, https://doi.org/10.1039/C5RA21000C

[66] Vanlalveni, C. *et al.*, Green synthesis of silver nanoparticles using plant extracts and their antimicrobial activities: a review of recent literature, *RSC Adv*., **2021**,11, 2804-2837, https://doi.org/10.1039/D0RA09941D

[67] Iravani, S. Green synthesis of metal nanoparticles using plants, *Green Chem*., **2011**,13, 2638-2650, https://doi.org/10.1039/C1GC15386B

[68] Jin, R. *et al.*, Photoinduced conversion of silver nanospheres to nanoprisms, Science, 2001, **294**, 1901-1903, https: DOI: 10.1126/science.1066541

[69] Sun, Y.; Yin,Y.; Mayers, B. T.; Herricks, T.; Xia, Y. Uniform Silver Nanowires Synthesis by Reducing AgNO3 with Ethylene Glycol in the Presence of Seeds and Poly(Vinyl Pyrrolidone), *Chem. Mater*., **2002,** 14, 4736–4745, https:// 10.1021/CM020587B

[70] Coskun, S.; Aksoy, B.; Unalan, H. E. Polyol Synthesis of Silver Nanowires: An Extensive Parametric Study, *Cryst. Growth Des.*, **2011**, 11, 4963–4969, https://doi.org/10.1021/cg200874g

[71] Pal, T.; Sau, T. K.; Jana, N. R. Redox Catalytic Properties of Palladium Nanoparticles: Surfactant and Electron Donor−Acceptor Effects, *Langmuir*, **1997**, 13, 1481–1485, https:// DOI:10.1021/la990507r

[72] Oliveira, M.J., Quaresma, P., Peixoto de Almeida, M. *et al.* Office paper decorated with silver nanostars - an alternative cost effective platform for trace analyte detection by SERS. *Sci. Rep.*, **2017**, **7**, 2480, https://doi.org/10.1038/s41598-017-02484-8

[73] Kumbhakar, P.; Biswas, S.; Tiwary, C. S.; Kumbhakar, P. Near white light emission and enhanced photocatalytic activity by tweaking surface defects of coaxial ZnO@ZnS core-shell nanorods, *J. Appl. Phys.*, **2017**, 121, 144301, https://doi.org/10.1063/1.4980011

[74] Xia, H.; Bai, S.; J. Hartmann and D. Wang, Synthesis of monodisperse quasi-spherical gold nanoparticles in water via silver(I)-assisted citrate reduction, *Langmuir*, **2010**, 26, 3585–3589, https://doi.org/10.1021/la902987w

[75] Steinigeweg, D.; Schlücker, S. Monodispersity and size control in the synthesis of 20–100 nm quasi-spherical silver nanoparticles by citrate and ascorbic acid reduction in glycerol–water mixtures, *Chem. Commun*., **2012**, 48, 8682-8684, https://doi.org/10.1039/C2CC33850E

[76] Li, H. *et al.*, Synthesis of Monodisperse, Quasi-Spherical Silver Nanoparticles with Sizes Defined by the Nature of Silver Precursors, *Langmuir*, **2014**, 30, 2498–2504, https:// DOI: 10.1021/la4047148

[77] Bastús, N. G.; Merkoçi, F.; Piella, J.; Puntes, V. Synthesis of Highly Monodisperse Citrate-Stabilized Silver Nanoparticles of up to 200 nm: Kinetic Control and Catalytic Properties, *Chem. Mater*., **2014**, 26, 2836–2846, https:// DOI:10.1021/cm500316k

[78] Choudhury, R,; Misra, T. K. Gluconate stabilized silver nanoparticles as a colorimetric sensor for Pb^{2+} , Colloids Surf. A: Physicochem. *Eng. Asp*., **2018**, 545, 179-187, https:// DOI:10.1016/j.colsurfa.2018.02.051

[79] Yu, D.; Yam, V. W. Controlled Synthesis of Monodisperse Silver Nanocubes in Water, *J. Am. Chem. Soc*., **2004**, 126, 13200–13201, https:// DOI: 10.1021/ja046037r

[80] Zhang, L. *et al.*, Kinetically controlled synthesis of large-scale morphology-tailored silver nanostructures at low temperature, *Nanoscale*, **2015**, **7**, 13420–13426, https://doi.org/10.1039/C5NR02611C

[81] Zhou. S. Facile Synthesis of Silver Nanocubes with Sharp Corners and Edges in an Aqueous Solution, *ACS Nano*, **2016**, 10, 9861–9870, https://doi.org/10.1021/acsnano.6b05776

[82] Pastoriza-Santos, I.; Liz-Marzán, L. M. Synthesis of Silver Nanoprisms in DMF, *Nano Lett*., **2002**, 2, 903–905, https:// DOI:10.1021/nl025638i

[83] Aherne, D.; Ledwith D. M.; Gara, M.; Kelly, J. M. Optical Properties and Growth Aspects of Silver Nanoprisms Produced by a Highly Reproducible and Rapid Synthesis at Room Temperature, *Adv. Funct. Mater*., **2008**, 18, 2005–2016, https://doi.org/10.1002/adfm.200800233

[84] Dong X.; Ji X.; Jing, J.; Li, M.; Li, J.; Yang, W. Synthesis of Triangular Silver Nanoprisms by Stepwise Reduction of Sodium Borohydride and Trisodium Citrate, *J. Phys. Chem. C*, **2010**, 114, 2070–2074, https:// DOI:10.1021/JP909964K

[85] Xu, X. *et al.*, Synthesis of triangular silver nanoprisms and studies on the interactions with human serum albumin, *J. Mol. Liq*., **2016**, 220, 14-20, https://doi.org/10.1016/j.molliq.2016.02.103

[86] Yakoh, A.; Rattanarat, P.; Siangproh, W.; Chailapakul, O. Simple and selective paper-based colorimetric sensor for determination of chloride ion in environmental samples using label-free silver nanoprisms, *Talanta***. 2018**, 178, 134-140,https:// DOI: 10.1016/j.talanta.2017.09.013

[87] Haber, J. M.; Sokolov, K. Dimensional Design for Surface-Enhanced Raman Spectroscopy, *Langmuir*, **2017**, 33, 10525–10530, https://doi.org/10.1021/acsmaterialsau.2c00005

[88] Dong, X. et al. Synthesis of Triangular Silver Nanoprisms by Stepwise Reduction of Sodium Borohydride and Trisodium Citrate, *J. Phys. Chem. C* **2010**, 114, 2070–2074, https://DOI:10.1021/jp909964k

[89] He, X.; Zhao, X. Solvothermal synthesis and formation mechanism of chain-like triangular silver nanoplate assemblies: Application to metal-enhanced fluorescence (MEF), *Appl. Surf. Sci*. **2009**, 255, 7361–7368, https://doi.org/10.1038/srep10196

[90] Guo, B. et al. 2D Layered Materials: Synthesis, Nonlinear Optical Properties, and Device Applications, *J Mater Sci: Mater Electron*., **2019**, 13, 625–630, https://doi.org/10.1002/lpor.201800327

[91] Jana, N. R.; Gearheart, L.; Murphy, C. J. Wet chemical synthesis of silver nanorods and nanowires of controllable aspect ratioElectronic supplementary information (ESI) available: UV–VIS spectra of silver nanorods, *Chem. Commun*., **2001**, 617, 617–618, https://doi.org/10.1039/B100521I

[92] Sun, Y.; Mayers, B.; Xia, Y. Size-Dependence of Surface Plasmon Resonance and Oxidation for Pd Nanocubes Synthesized via a Seed Etching Process, *Nano Lett*., **2003,**3, 5, https://DOI: 10.1021/nl0508826

[93] Zhang, D.; Qi, L.; Yang, J.; Ma, J.; Cheng, H.; Huang, L. Wet Chemical Synthesis of Silver Nanowire Thin Films at Ambient Temperature, *Chem. Mater*. **2004**, 16, 872-876, https://doi.org/10.1021/cm0350737

[94] X. Gu, C. Nie, Y. Lai, C. Lin, Synthesis of silver nanorods and nanowires by tartrate-reduced route in aqueous solutions, *Mater. Chem. Phys*. **2006**, 96, 217–222, https://DOI:10.1016/j.matchemphys.2005.07.006

[95] A. Roy *et al.*, Directional growth of Ag nanorod from polymeric silver cyanide: A potential substrate for concentration dependent SERS signal enhancement leading to melamine detection, *Spectrochim. Acta A Mol. Biomol. Spectrosc*.**,** **2017**, 183, 402–407, https://doi.org/10.1016/j.saa.2017.04.074

[96] M. B. Gebeyehu, T. F. Chala, S. Y. Chang, C. Wu and J. Lee, Synthesis and highly effective purification of silver nanowires to enhance transmittance at low sheet resistance with simple polyol and scalable selective precipitation method, *RSC Adv*., **2017**, **7**, 16139-16148, https://doi.org/10.1039/C7RA00238F

[97] H. Xu *et al.*, Synthesis of high-purity silver nanorods with tunable plasmonic properties and sensor behavior, *Photon. Res.* **2017**, 5, 27-32, https://doi.org/10.1364/PRJ.5.000027

[98] J. Xu, J. Hu, C. Peng, H. Liu, Y. Hu, A simple approach to the synthesis of silver nanowires by hydrothermal process in the presence of gemini surfactant, *J. Colloids and Interface Sci*., **2006**, 298, 689–693, https//DOI: 10.1016/j.jcis.2005.12.047

[99] D. Chen, X. Qiao, X. Qiu, J. Chen and R. Jiang, Synthesis and electrical properties of uniform silver nanoparticles for electronic applications, *J. Colloid and Interface Sci*., **2010**, 344, 286–291, https://DOI:10.1007/s10853-008-3204-y

[100] B. K. Jena, B. K. Mishra and S. Bohidar, Controlled Synthesis of Monodisperse Silver Nanocubes in Water, *J. Phys. Chem. C*, 113, 33, 14753-14758, https://doi.org/10.1039/D3NA00163F

[101] H. Liang, Z. Li, W. Wang, Y. Wu and H. Xu, Highly Surface-roughened "Flower-like" Silver Nanoparticles for Extremely Sensitive Substrates of Surface-enhanced Raman Scattering, *Adv. Mater*. **2009**, 21, 4614–4618, https:// DOI:10.3390/nano11123184

[102] A. Pourjavadi and R. Soleyman, Novel silver nano-wedges for killing microorganisms, *Mater. Res. Bull*. **2011**, 46, 1860–1865, https://doi.org/10.1016/j.materresbull.2011.07.040

[103] S. Roy, C. M. Ajmal, S. Baik and J.Kim, Silver nanoflowers for single-particle SERS with 10 pM sensitivity, *Nanotechnology*, **2017**, 28, 465705-465728, https://doi: 10.1088/1361-6528/aa8c57.

[104] P. Yang, J. Zheng, Y. Xu, Q. Zhang, L. Jiang, Colloidal Synthesis and Applications of Plasmonic Metal Nanoparticles, *Adv. Mater*. **2016,** 28, 10508-10517, https://doi.org/10.1002/adma.201601739

[105] Q. Zhang, Y. N. Tan, J. Xie, J. Y. Lee, Colloidal Synthesis of Plasmonic Metallic Nanoparticles, *Plasmonics*, **2009,** 4, 9–22, https://doi.org/10.1007/s11468-008-9067-x

[106] R. Becker and W. Döring, Kinetic treatment of nucleation in supersaturated vapors, *Ann. Phys*., **1935**, 24, 719–752.

[107] V. K. LaMer and R. H. Dinegar, Theory, Production and Mechanism of Formation of Monodispersed Hydrosols, *J. Am. Chem. Soc*., **1950**, 72, 4847–4854, https://doi.org/10.1021/ja01167a001

[108] J. Polte, Fundamental growth principles of colloidal metal nanoparticles – a new perspective, Cryst. *Eng. Comm*, 2015, **17**, 6809–6830, https://doi.org/10.1039/C5CE01014D

[109] Y. Jun, D. Kim and C. W. Neil, Heterogeneous Nucleation and Growth of Nanoparticles at Environmental Interfaces, *Acc. Chem. Res*., **2016,** 49, 1681–1690, https://doi.org/10.1021/acs.accounts.6b00208

[110] V. K. LaMer, Kinetics and Mechanisms of Aggregative Nanocrystal Growth, *Ind. Eng. Chem*., **1952**, 44, 1270–1277, https://doi.org/10.1021/cm402139r

[111] S. T. Gentry, S.F. Kendra and M. W. Bezpalko, Nanocrystalline graphene at high temperatures: insight into nanoscale processes, *J. Phys. Chem. C*, **2011**, 115, 12736–12741, DOI https://doi.org/10.1039/C9NA00055K

[112] B. Ingham *et al.*, How Nanoparticles Coalesce: An in Situ Study of Au Nanoparticle Aggregation and Grain Growth, *Chem. Mater*., **2011**, 23, 3312–3317, https://doi.org/10.1021/cm200354d

[113] S. E. H. Murph, C. J. Murphy, A. Leach and K. Gall, A possible oriented attachment growth mechanism for silver nanowire formation, *Cryst. Growth Des*., **2015,** 15, 1968–1974, https://DOI:10.1021/acs.cgd.5b00123

[114] M. S. Bakshi, How surfactants control crystal growth of nanomaterials, *Cryst. Growth Des*., 2016, **16**, 1104–1133, https:// DOI:10.1021/acs.cgd.5b01465

[115] K. M. Koczkur, S. Mourdikoudis, L. Polavarapu and S. E. Skrabalak, Polyvinylpyrrolidone (PVP) in nanoparticle synthesis, *Dalton Transac*., **2015,** 44, 17883-17905, https://doi.org/10.1039/C5DT02964C

[116] X. Xia, J. Zeng, Q. Zhang, C. H. Moran and Y. Xia. Recent Developments in Shape-Controlled Synthesis of Silver Nanocrystals, *J. Phys. Chem. C Nanomater. Interfaces*., **2012**, 116, 21647–21656, https:// DOI: 10.1021/jp306063p

[117] H. Wang, X. Qiao, J. Chena, X. Wang and S. Ding, Mechanisms of PVP in the preparation of silver nanoparticles, Mater. Chem. Phys. **2005**, 94, 449-453, https:// DOI:10.1007/s11051-014-2723-5

[118] R. Mehra, Application of refractive index mixing rules in binary systems of hexadecane and heptadecane withn-alkanols at different temperatures, Proc. Indian Acad. Sci. (Chem. Sci.) **2003**, 115, 147-154, https://doi.org/10.1007/BF02716982

[119] X. C. Jiang, W. M. Chen, C. Y. Chen, S. X.Xiong and A. B. Yu, Role of temperature in the growth of silver nanoparticles through a synergetic reduction approach, Nanoscale Res. Lett., **2011**, 6, 32-40, https://doi.org/10.1039/D0NA01013H

[120] H. Chen *et al.*, Structural properties of silver nanorods with fivefold symmetry, Micron., **2004**, 35, 469–474, https://doi.org/10.1016/j.micron.2004.02.008

[121] Q. Yu *et al.*, Strong crystal size effect on deformation twinning, Nature, **2010**, 463, 335–343, https:// DOI: 10.1038/nature08692

[122] F. Baletto and R. Ferrando, Structural properties of nanoclusters: Energetic, thermodynamic, and kinetic effects, Rev. Mod. Phys., **2005,** 77, 371–423, https://doi.org/10.1103/RevModPhys.77.371

[123] B. Wiley, Y. Sun and Y. N. Xia, Synthesis of Silver Nanostructures with Controlled Shapes and Properties, Acc. Chem. Res., **2007**, 40,1067–1076, https:// DOI: 10.1021/ar7000974

[124] J. Jana, M. Ganguly and T. Pal, Enlightening surface plasmon resonance effect of metal nanoparticles for practical spectroscopic application, RSC Adv., **2016**, 6, 86174-86211, https://doi.org/10.1039/C6RA14173K

[125] M. A. Garcia, J. Phys. D: Appl. Phys., Surface plasmons in metallic nanoparticles: fundamentals and applications, **2011,** 44, 283001-283021, https://DOI:10.1088/0022-3727/44/28/283001

[126] C. Noguez, Surface Plasmons on Metal Nanoparticles: The Influence of Shape and Physical Environment, J. Phys. Chem. C, **2007,** 111, 3806–3819, https://doi.org/10.1021/jp066539m

[127] G. Mie, Contributions to the Optics of Turbid Media, Particularly of Colloidal Metal solutions, *Ann. Phys*., **1908**, 25, 377-445, https://doi.org/10.1002/andp.19083300302

[128] A. Alabastri et al., Molding of Plasmonic Resonances in Metallic Nanostructures: Dependence of the Non-Linear Electric Permittivity on System Size and Temperature, Materials, **2013**, 6, 4879-4910, https://doi.org/10.3390/ma6114879

[129] U. Kreibig and M. Vollmer, Optical properties of metal clusters. Springer; Berlin: **1995**, https://doi.org/10.1007/978-3-662-09109-8

[130] R. Gans, about the shape of ultramicroscopic gold particles, Annalen der Physik, **1912**, 342, 881-900, http://dx.doi.org/10.1002/andp.19123420503

[131] S. Link and M. El-Sayed, Simulation of the Optical Absorption Spectra of Gold Nanorods as a Function of Their Aspect Ratio and the Effect of the Medium Dielectric Constant, J. Phys. Chem. B, **2005**, 109, 10531-10532, https://doi.org/10.1021/jp058091f

[132] S. Borja, C. A. Paula, M. L. Laura and M. L. Luis, Effect of the Dielectric Properties of Substrates on the Scattering Patterns of Gold Nanorods, Nano Today, **2009**, 4, 244–251, https:// DOI:10.1021/nn200951c

[133] O. A. Yeshchenko, I. S. Bondarchuk, Y. M. Losytskyy, A. A. Alexeenko, Low-Temperature Plasmonics of Metallic Nanostructures, Plasmonics, **2014,** 9, 93–101, https:// DOI:10.1007/978-3-030-18834-4_11